IEEE Access
Multidisciplinary ⋮ Rapid Review ⋮ Open Access Journal

Received 17 April 2024, accepted 19 May 2024, date of publication 27 May 2024, date of current version 6 June 2024.

Digital Object Identifier 10.1109/ACCESS.2024.3406209

RESEARCH ARTICLE

Super-Resolution Correlating Optical Endoscopy

OSKAR TAMM[1], VIPIN TIWARI[1], SHIVASUBRAMANIAN GOPINATH[1], ARAVIND SIMON JOHN FRANCIS RAJESWARY[1], SCOTT AROCKIA SINGH[2,3], JOSEPH ROSEN[1,4], AND VIJAYAKUMAR ANAND[1,5]

[1]Institute of Physics, University of Tartu, 50411 Tartu, Estonia
[2]Dr. Jeyasekharan Hospital, Nagercoil, Tamil Nadu 629003, India
[3]Dr. Scott's Laser Piles, Fistula Laparoscopic Center, Nagercoil, Tamil Nadu 629201, India
[4]School of Electrical and Computer Engineering, Ben Gurion University of the Negev, Be'er-Sheva 8410501, Israel
[5]Optical Sciences Center, School of Science, Computing and Engineering Technologies, Swinburne University of Technology, Hawthorn, Melbourne, VIC 3122, Australia

Corresponding author: Vijayakumar Anand (vijayakumar.anand@ut.ee)

This work was supported in part by European Union's Horizon 2020 Research and Innovation Programme from Australian Research Council through Computational Imaging and Processing in High Resolution (CIPHR) under Grant 857627 and Grant DP240103231, and in part by Israel Innovation Authority under MAGNET under Grant 79555.

ABSTRACT Optical endoscopy is a widely used minimally invasive diagnostic tool for imaging internal organs. The imaging resolution is defined by the numerical aperture of the objective lens. In this study, we proposed and demonstrated a Super-resolution Correlating OPtical Endoscopy (SCOPE) system. In SCOPE, modified recording and reconstruction methods are introduced with the existing built-in endoscopy lens. Instead of recording a single image, multiple images of the object are recorded by scanning the tip of the endoscope around the object. The recorded low-resolution images of the object are arranged as sub-matrices in a 2D matrix. Another similar 2D matrix with either recorded or synthesized point spread functions (PSFs) is created. The 2D matrices of the object and the PSF were processed using a deconvolution algorithm to reconstruct a super-resolution image of the object. Both simulation and proof-of-concept experimental studies have been presented. SCOPE neither requires any additional optical element nor any changes in the endoscopy system itself; therefore, it can be easily implemented in commercial endoscopy systems.

INDEX TERMS Indirect imaging, coded aperture correlation holography, endoscopy, microscopy, imaging, super-resolution.

I. INTRODUCTION

Endoscopy is a versatile tool used by modern-day physicians for imaging and surgery of internal organs [1]. Like most commercial imaging systems, endoscopy uses a direct mode of imaging for recording object information [2], [3]. In direct imaging mode, the light from an object is collected and focused by a refractive lens on an image sensor and/or the eye with image formation governed by the conventional laws of optics [4]. The lateral resolution of imaging is given as $\sim \lambda/NA$, where NA is the numerical aperture given approximately as $D/2u$, where D is the diameter of the objective lens and u is the distance of the object from the lens. In the case of a single lens imaging system $u = \left(1/f - 1/v\right)^{-1}$, where f is the lens focal length, and v is the distance of the detection plane from the lens. In recent years, several attempts have been made to improve endoscopy technology beyond the conventional imaging framework [5], [6], [7], [8], [9], [10]. In most commercial endoscopy systems, the light source and image sensor are part of the probing unit entering the body. The sample is illuminated by the light source and directly recorded by the image sensor. The recorded signal is transmitted as an electronic signal to the computer through electrical cables. In [9] and [10], an ultrathin endoscopy system was realized by moving the image sensor and light source out of the probing unit. Since the object information

The associate editor coordinating the review of this manuscript and approving it for publication was Chao Zuo.

© 2024 The Authors. This work is licensed under a Creative Commons Attribution-NonCommercial-NoDerivatives 4.0 License.
For more information, see https://creativecommons.org/licenses/by-nc-nd/4.0/

is transferred through an optical fibre, the image of the object can be obtained only after computational processing of the recorded distributions. In [9] and [10], deep learning and computational algorithms, respectively, were used to obtain object information. While the above developments will enable moving beyond the state-of-the-art of modern-day endoscopy systems, implementing them requires fundamental changes to the existing endoscopy architecture, which may be a burden on the industry without evidence of substantial improvements.

In recent years, interferenceless coded aperture correlation holography (I-COACH), a new sub-field of imaging, has been growing rapidly and is emerging as a technology for the future [11]. The I-COACH imaging technique is an indirect imaging technique consisting of at least two steps: optical recording and computational reconstruction. In the optical recording step, instead of the image of an object, a distorted projection of the object is recorded. In the computational reconstruction step, the image of the object is reconstructed with additional information that cannot be obtained through direct imaging. Many imaging techniques developed based on the foundations of I-COACH with capabilities beyond the conventional limits in several imaging dimensions, resolution, field of view, etc., are thoroughly reviewed in [12], [13], and [14].

Multiple developments in the I-COACH technique, such as aperture engineering and reconstruction methods, have been made. The first version of I-COACH used scattering masks, while the latest version used cubic phase masks, and the above requirements of special masks constrict wider implementation [12], [13], [14]. A super-resolution endoscopy system based on I-COACH was reported [15] that used a modified endoscope configuration with a ring-shaped coded aperture. Recently, I-COACH was also demonstrated directly on an infrared microscope with a microscopic objective, such as a coded mask [16]. Based on the above study, I-COACH was applied to a direct lens-based imaging system, and an improvement in the lateral resolving power beyond the limit of the NA was observed [17], [18].

In this study, we propose and demonstrate a Super-resolution Correlating OPtical Endoscopy (SCOPE) system based on I-COACH and the understanding gained from recent implementations [15], [17], [18]. In SCOPE, multiple recordings of an object are made using a regular endoscopy system by scanning the tip of the endoscope around the object. The recorded images are arranged in a 2D matrix and processed with an identical matrix consisting of the recordings of a point using a deconvolution algorithm [19]. The reconstructed image has an improved resolution compared to the individual recording with a higher signal-to-noise ratio. This approach does not require fundamental changes in the architecture of the endoscopy system, as in [9], [10], and [15], and therefore can be easily implemented with existing commercial endoscopy systems.

The manuscript consists of five sections. The theory of SCOPE is presented in the next section. The simulation studies are presented in the third section. Proof-of-concept experimental studies are presented in the fourth section. The results and the pathway for implementing SCOPE in existing commercial endoscopy systems are discussed in the fifth section. The conclusion and future perspectives are presented in the final section.

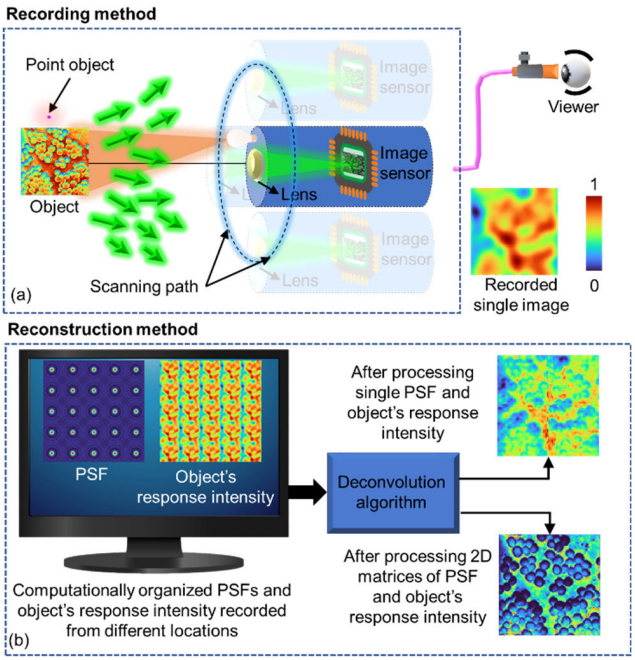

FIGURE 1. (a) Optical recording configuration of SCOPE. (b) Computational reconstruction configuration of SCOPE.

II. METHODS

The SCOPE configuration of optical recording and computational reconstruction is shown in Figure 1. Commercial endoscopy systems are sophisticated, with many variations and options depending upon the required application. The length of the probing unit can vary between a few centimeters and a few meters, and the diameter can vary from a few millimeters to an inch depending upon the type of physical body of the animal, which can vary from small to large. For the diagnosis of human organs, standard sizes of endoscopes and colonoscopies are manufactured. Depending upon the application, endoscopy systems can have only one imaging unit or several units with biopsy and treatment modules. Figure 1 shows a simple configuration of an imaging unit consisting of an illumination source, a lens and an image sensor. An object is recorded, and a point object is optionally recorded. The point spread function (PSF) can be obtained by a recording, extracted from the object's response intensity or synthesized depending upon the restrictions around the sample. In this study, the PSF was recorded. The imaging procedure involves multiple recordings of the point object and object by scanning the tip of the endoscope around the object. The recorded object intensity and PSFs are arranged as submatrices in a large matrix and processed using one of the deconvolution

methods discussed in [19]. The computational reconstruction generates an image with a lateral resolution higher than that of the directly recorded image and reconstructed image with a single recording using a deconvolution algorithm, as shown in Figure 1. In this study, only spatially incoherent illumination was considered because only such light sources are used in commercial endoscopy systems. Therefore, the theoretical analysis is performed for a single point and extended directly to a 2D object by a mathematical convolution operation. A free space optical configuration with object and image distances z_s and z_h and a lens with a focal length f mimicking SCOPE is shown in Figure 2, which is used for theoretical analysis and experimental demonstration.

An isolated point object with an amplitude of $\sqrt{I_s}$ located at $\bar{r}_s=(x_s, y_s)$ is considered. The point object is axially at a distance of z_s from the imaging lens with a diameter of D_2 that can move inside a circle with a diameter of D_1. The complex amplitude reaching the refractive lens is given as $C_1\sqrt{I_s}L\left(\frac{\bar{r}_s}{z_s}\right)Q\left(\frac{1}{z_s}\right)$, where $L\left(\frac{\bar{s}}{z_s}\right) = \exp\left[\frac{j2\pi(s_x x+s_y y)}{\lambda z_s}\right]$ is a linear phase function, $Q(b)=\exp\left[j\frac{\pi b}{\lambda}\left(x^2+y^2\right)\right]$ is a quadratic phase function and C_1 is a complex constant. It must be noted that even though the proposed method is an indirect imaging method, every recording is made under direct imaging mode satisfying the equation $f = \left(\frac{1}{z_s}+\frac{1}{z_h}\right)^{-1}$. The lens function is given as $Q_{Lens}\left(-\frac{1}{f}\right)=\exp\left[-j\frac{\pi}{\lambda f}\left((x-a_x)^2+\left(y-a_y\right)^2\right)\right]$ $Circ\left(D_2/2\right)$, where $\left(a_x, a_y\right)$ is the transverse location of the center of the lens and

$$Circ\left(D_2/2\right)=\begin{cases}1, & \text{for} \quad 0<\sqrt{(x-a_x)^2+\left(y-a_y\right)^2}\\ & \leq D_2/2\\ 0, & elsewhere\end{cases}$$

is a top-hat function that is 1 within the circle of radius $D_2/2$ and 0 elsewhere, and $0 \leq \left(a_x, a_y\right) \leq \left(\frac{D_1}{2}-\frac{D_2}{2}\right)$. The complex amplitude after the refractive lens is given as $C_1\sqrt{I_s}L\left(\frac{\bar{r}_s}{z_s}\right)Q\left(\frac{1}{z_s}\right)Q_{Lens}\left(-\frac{1}{f}\right)$ for $\left(a_x=0, a_y=0\right)$. Substituting z_h for z_s and f, we obtain the simplified complex amplitude after the lens as $C_1\sqrt{I_s}L(\bar{r}_s/z_s)Q\left(-1/z_h\right)$. The intensity distribution at a distance of z_h from the refractive lens is given as

$$I_{PSF}\left(\bar{r}_o;\bar{r}_s\right)=\left|C_2\sqrt{I_s}Q\left(-\frac{1}{z_h}\right)L\left(\frac{\bar{r}_s}{z_s}\right)\otimes Q\left(\frac{1}{z_h}\right)\right|^2, \tag{1}$$

which reduces to a delta-like function with a width of $\sim 2\lambda z_h/D_2$ in the sensor plane and a location given by the linear phases associated with location $\bar{r}_s$ and magnification $M = z_h/z_s$, where '$\otimes$' is a 2D convolutional operator. The above equation can be modified as

$$I_{PSF}\left(\bar{r}_o;\bar{r}_s\right)=I_{PSF}\left(\bar{r}_o-\frac{z_h}{z_s}\bar{r}_s;0\right). \tag{2}$$

A 2D object can be considered a collection of points given as

$$o\left(\bar{r}_s\right)=\sum\nolimits_i b_i\delta\left(\bar{r}_s-\bar{r}_i\right). \tag{3}$$

The intensity of the object's response at the image sensor is given as

$$I_o\left(\bar{r}_o\right)=\sum\nolimits_i b_i I_{PSF}\left(\bar{r}_o-\frac{z_h}{z_s}\bar{r}_s;0\right). \tag{4}$$

The image of the object can be reconstructed using a cross-correlation given as

$$\begin{aligned}P\left(\bar{r}_R\right)&=\int\int I_o\left(\bar{r}_o\right)I^*_{PSF}\left(\bar{r}_o-\bar{r}_R\right)d\bar{r}_0\\&=\int\int\sum_i b_i I_{PSF}\left(\bar{r}_o-\frac{z_h}{z_s}\bar{r}_{s,i}\right)I^*_{PSF}\left(\bar{r}_o-\bar{r}_R\right)d\bar{r}_0\\&=\sum\nolimits_i b_i\Lambda\left(\bar{r}_R-\frac{z_h}{z_s}\bar{r}_{s,i}\right)\approx o\left(\frac{z_s}{z_h}\bar{r}_R\right),\end{aligned} \tag{5}$$

where Λ is a delta-like function with a width of $\sim 2\lambda z_s/D_2$ in the image plane.

In SCOPE, instead of I_{PSF}, a synthetic PSF given as I_{SPSF} is obtained by accumulating the I_{PSF} for different values of a_x and a_y and summing them where each is positioned at $\bar{a} = \left(a_x, a_y\right)$. The I_{SPSF} is given as

$$I_{SPSF}=\sum\nolimits_{a_x,a_y} I_{PSF}\left(\bar{r}_o-\bar{a};0\right). \tag{6}$$

The synthetic object intensity distribution is given as

$$I_{SO}=\sum\nolimits_{a_x,a_y} I_o\left(\bar{r}_o-\bar{a};0\right). \tag{7}$$

From Eq. (5), Eq. (7) can be modified as

$$I_{SO}=\sum\nolimits_{a_x,a_y}\sum\nolimits_i b_i I_{PSF}\left(\bar{r}_o-\frac{z_h}{z_s}\bar{r}_{s,i}-\bar{a}\right) \tag{8}$$

The super-resolution image of the object can be reconstructed by correlating I_{SPSF} and I_{SO}, as shown in Eq. (5), which can also be expressed simply as $O_R = I_{SO} * I_{SPSF}$, where '$*$' is a 2D correlation operator. The reconstructed points have a delta-like shape with a width of $\sim 2\lambda z_s/D_2$ in the image plane. The correlation operation can be achieved using one of the many available computational algorithms [19].

The resolution improvement is achieved due to the deconvolution, first at the level of a single recording [20] and then at the level of the array of multiple recordings. A single recording image is expressed as

$$I_o\left(\bar{r}_o\right)=o\left(\bar{r}_o\right)\otimes I_{PSF}\left(\bar{r}_o\right)+n\left(\bar{r}_o\right), \tag{9}$$

where $n\left(\bar{r}_o\right)$ is the detection noise. The deconvolution process of the Lucy-Richardson-Rosen algorithm (LRRA) [16], [17], [18] used herein magnifies the high frequencies inside the spectral bandwidth. Therefore, because the fine details of an object are represented mostly in the high frequencies of the spatial spectrum, the image resolution is enhanced, but the noise is also magnified. The reconstructed image $I_R\left(\bar{r}_o\right)$

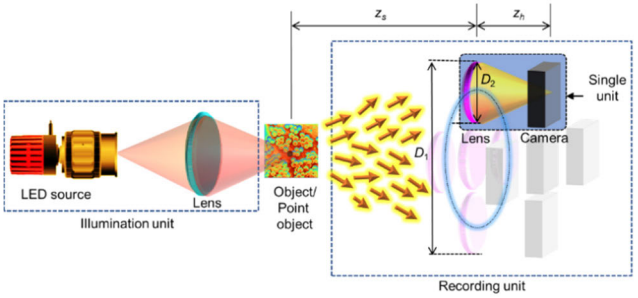

FIGURE 2. Free space optical configuration for mimicking SCOPE.

obtained by deconvolution can be effectively described as a single iteration of spatial filtering as follows:

$$I_R(\bar{r}_o) = [o(\bar{r}_o) \otimes I_{PSF}(\bar{r}_o) + n(\bar{r}_o)] * \tilde{I}_{PSF}(\bar{r}_o) \cong o(\bar{r}_o) + n(\bar{r}_o) * \tilde{I}_{PSF}(\bar{r}_o), \quad (10)$$

where $\tilde{I}_{PSF}(\bar{r}_o)$ is the deconvolution function computed upon the information of $I_{PSF}(\bar{r}_o)$ [19]. According to the results of Eq. (10), for a single recording, a noise term is added to the improved resolution image. Assuming that the noise term $n(\bar{r}_o) * \tilde{I}_{PSF}(\bar{r}_o)$ has a zero mean, multiple independent deconvolution events can reduce the noise. Multiple recordings at different times guarantee multiple independent events of detection noise added to the recorded images. Hence, an array of independent noise functions is added to the synthetic object intensity of Eq. (8). Therefore, the reconstructed image is

$$\begin{aligned} I_R(\bar{r}_o) &= \left[I_{SO} + \sum\nolimits_{a_x,a_y} n(\bar{r}_o - \bar{a}) \right] * \tilde{I}_{SPSF}(\bar{r}_o) \\ &\cong o(\bar{r}_o) + \left[\sum\nolimits_{a_x,a_y} n(\bar{r}_o - \bar{a}) \right] * \tilde{I}_{SPSF}(\bar{r}_o) \\ &= o(\bar{r}_o) + \sum\nolimits_{a_x,a_y} n(\bar{r}_o - \bar{a}) * I_{PSF}(\bar{r}_o - \bar{a}; 0) \\ &\cong o(\bar{r}_o), \end{aligned} \quad (11)$$

where $\tilde{I}_{SPSF}(\bar{r}_o)$ is the deconvolution function in the shape of an array of PSFs computed upon the information of $I_{SPSF}(\bar{r}_o)$. The noise term in the second line of Eq. (11) is approximately zero based on the assumption that each term of $n(\bar{r}_o - \bar{a}) * \tilde{I}_{PSF}(\bar{r}_o - \bar{a})$ for every a_x, a_yhas a zero mean.

III. SIMULATION STUDIES

Computer simulation was carried out in MATLAB with a matrix size of 500 × 500 pixels, pixel size $\Delta = 10\ \mu$m, and wavelength $\lambda = 650$ nm. A sub-matrix window with a size of 100 × 100 pixels was used for scanning over the 500 × 500 pixel matrix with a step size of 100 pixels. The object and image distances were set as $z_s = 80$ cm and $z_h = 26.7$ cm to satisfy the imaging equation for a lens with a focal length $f = 20$ cm. Fresnel propagators have been used to verify this idea, and therefore, the distances are larger. However, by changing Δ, λ and distances, the simulation results can be scaled to different distances and wavelengths. For this

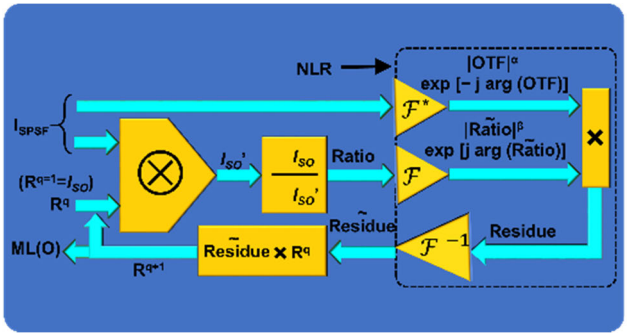

FIGURE 3. Schematic of the Lucy–Richardson–Rosen algorithm. OTF – optical transfer function; q—number of iterations of LRRA; ⊗—2D convolutional operator; R^q is the qth solution; and q is an integer; when $q = 1$, $R^q = I_O$; and α and β are varied from −1 to 1; ∼ - Fourier Transform, ∗ complex conjugate; NLR is a nonlinear reconstruction; $\mathcal{F}$ and $\mathcal{F}^{-1}$ are Fourier and inverse Fourier transforms, respectively.

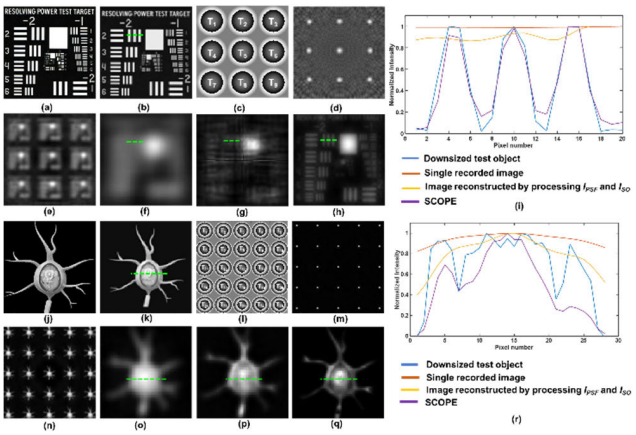

FIGURE 4. Simulation results: (a) Binary test object. (b) Downsize binary test object. (c) Accumulated phase obtained by scanning the lens and camera unit at T_1 to T_9. (d) I_{SPSF}, (e) I_{SO}, (f) single recorded image, and (g) image reconstructed by processing I_{PSF} and I_{SO}. (h) SCOPE reconstruction, (i) line plot (lateral profile) for the region of interest (ROI) for Figure 4 (b, f, g, h) (the green dashed line shows the data extraction location of the line plot. (j) Grayscale test object. (k) Downsize grayscale test object. (l) Accumulated phase obtained by scanning the lens and camera unit at T_1 to T_{25}. (m) I_{SPSF}, (n) I_{SO}, (o) single recorded image, and (p) image reconstructed by processing I_{PSF} and I_{SO}. (q) SCOPE reconstruction and (r) line plot (lateral profile) for the ROI in Figure 4 (k, o, p, q) (the green dashed line shows the data extraction location of the line plot).

study, LRRA was used for image reconstruction, as shown in Figure 3. A binary USAF object image was used as the test object for the simulation studies, as shown in Figure 4(a). The test object was downsized to a reduced number of pixels for simulation, as shown in Figure 4(b). A total of 9 recordings in a 3 × 3 configuration were simulated for the I_{PSF} and I_O. Images of the accumulated phase functions of the lens, I_{SPSF} and I_{SO} are shown in Figures 4(c)-4(e), respectively. The magnified single recording, reconstruction by processing I_{PSF} and I_O and reconstruction by processing I_{SPSF} and I_{SO} are shown in Figures 4(f)-4(h), respectively [16]. The line plots (lateral profiles) of the region of interest (ROI) in Figures 4 (b, f, g, h) are shown in Figure 4(i). In the next step, SCOPE was simulated for a grayscale test object

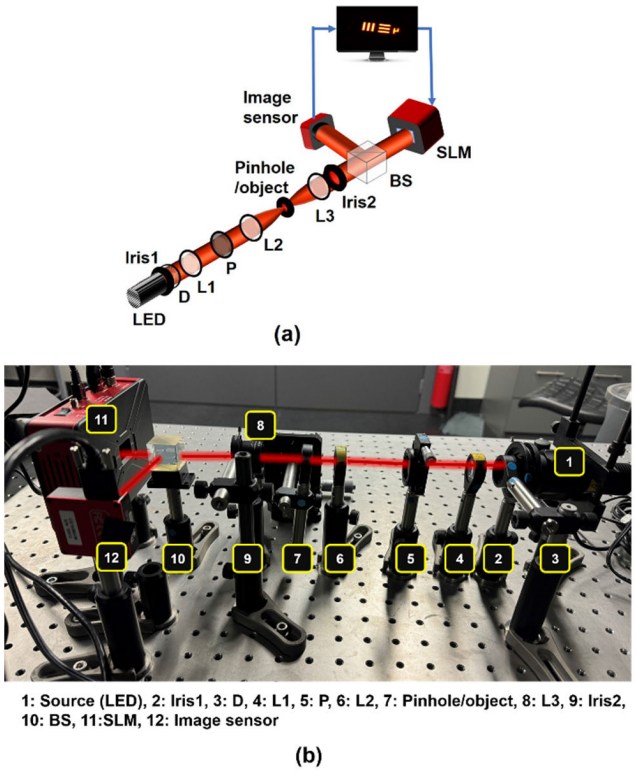

FIGURE 5. Experimental configuration of SCOPE. (a) Schematic of the experimental setup and (b) photograph of the experimental setup. [LED: Light Emitting Diode, D: Diffuser, Ln (n=1,2,3): Lens, BS: Beam Splitter, SLM: Spatial Light Modulator].

(a neuron image) and a downsized test object, as shown in Figure 4(j, k) respectively. In this case, the object and image distances were set as $z_s = 100$ cm and $z_h = 11.11$ cm to satisfy the imaging equation for a lens with a focal length $f = 10$ cm. A total of 25 recordings arranged in a 5×5 configuration were simulated for the I_{PSF} and I_O. Images of the accumulated phase functions of the lens, I_{SPSF} and I_{SO} are shown in Figures 4(l)-4(n), respectively. The magnified single recording, reconstruction by processing I_{PSF} and I_O and reconstruction by processing I_{SPSF} and I_{SO} are shown in Figures 4(o)-4(q), respectively. The line plot (lateral profile) of the ROIs in Figures 4 (k, o, p, q) are shown in Figure 4(r). The LRRA was operated with the following conditions ($\alpha = 0$, $0.5 \leq \beta \leq 0.7$, $4 \leq n \leq 7$), where n is the number of iterations. As seen from the simulation results, with SCOPE, the image resolution can be significantly improved, and the improvement is proportional to the number of recordings.

IV. EXPERIMENTS

Figure 5(a) shows a schematic of the experimental configuration of SCOPE, and a photograph of the experimental setup is shown in Figure 5(b). A red-light beam emanating from a high-power LED (Thorlabs, 940 mW, $\lambda = 660$ nm and $\Delta\lambda = 20$ nm, Newton, MA, USA) is collimated by a refractive lens (L1) with a focal length of 50 mm. An iris1 and a diffuser (D) (Thorlabs Ø1" Ground Glass Diffuser-220 GRIT, Newton, MA, USA) are used to control the initial beam illumination and to remove the grating lines of the LED, respectively. This collimated beam is passed through a linear polarizer (P) oriented along the active axis of the SLM. An object is critically illuminated using a converging lens (L2) with a focal length of 50 mm. Light from the object is then collected by a collimating lens (L3) with a focal length of 50 mm and an iris2. The collimated beam was incident on an SLM (Thorlabs Exulus HD2, 1920 × 1200 pixels, pixel size = 8 μm, Newton, MA, USA) through a beam splitter (BS). Light reflected from the SLM is directed to an image sensor (Zelux CS165MU/M 1.6 MP monochrome CMOS camera, 1440 × 1080 pixels with a pixel size of ~3.5 μm; Newton, MA, USA), which is placed at the reflecting arm of the BS at a distance of 178 mm from the SLM.

In the experiment, a pinhole with a diameter of 25 μm was used to record the I_{PSF} in the image sensor. Three objects, O1: two points (25 μm each, 20 μm apart) and O2: two gratings (horizontal and vertical) with digit 4 from Group 4 of R1DS1N—Negative 1951 USAF Test Target, Ø1"), and O3 (insect wing) were used in this experiment.

In the first step, SCOPE was tested for simple object O1, i.e., two points (each with a size of 25 μm and a distance of 20 μm). The lens array mask (LAM) for SCOPE was designed by stitching 3×3=9 subapertures (~55 SLM pixels each) and was displayed on SLM. The PSF and the corresponding object response intensities (ORIs) were recorded. In addition, the PSF and ORI were also recorded for a Diffractive Lens Mask (DLM) with a focal length of 178 mm with a Combined Aperture Mask (CAM), which is a DLM but with the same aperture size as the LAM. Figure 6(a-d) shows the (a) CAM (3×3), (b) LAM (3×3), (c) recorded PSF for the LAM, and (d) ORI for the LAM. The direct images recorded via regular endoscopy for the CAM (DICAM) and ORI for a single element of the LAM are presented in Figures 6(e, f), respectively. The reconstruction results for regular endoscope imaging and SCOPE for O1 using LRRA are depicted in Figure 6(g, h). For visibility comparison, a line plot is shown for the highlighted region of Figure 6(e-h) in Figure 6(i). A comparison of figures 6(e-h) shows that two points are best resolved for SCOPE. Furthermore, the full width at half maximum (FWHM) was calculated from the plots in Figure 6 (i) and is shown in Figure 6 (j). The minimum value of the FWHM was obtained in SCOPE compared to the other methods, which demonstrates enhanced resolution.

In the next experiment, the feasibility of SCOPE was tested for multi-element object O2 (Group 4 elements of 1DS1N—Negative 1951 USAF Test Target, Ø1"). Similarly, the PSFs and ORIs were recorded for O2. In this case, the LAM for SCOPE was designed by stitching 4×4=16 subapertures (~55 SLM pixels each) and was displayed on the SLM. Figure 7(a-d) shows the (a) CAM (4×4), (b) LAM (4×4), (c) recorded PSF for the LAM, and (d) ORI for the LAM. The recorded ORIs for the CAM and ORI for direct recording via regular endoscopy are presented in Figures 7(e, f), respectively. The reconstruction results for

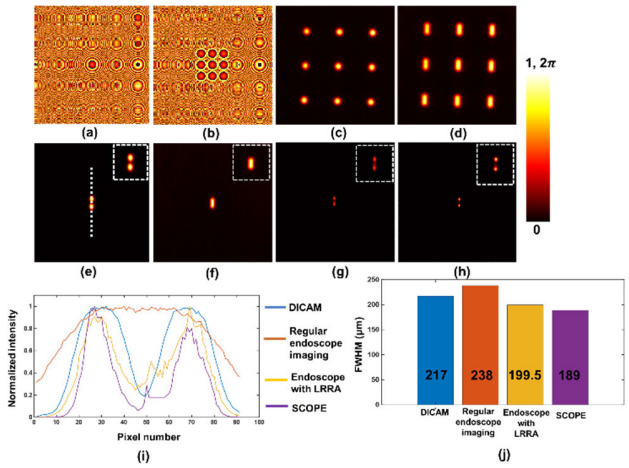

FIGURE 6. Experimental results for Object1 (O1). (a) CAM (3 × 3), (b) LAM (3 × 3), (c) recorded PSF using LAM, (d) recorded ORI using LAM, (e) ORI using CAM, (f) ORI for regular endoscope, (g) regular endoscope using LRRA, (h) SCOPE using LRRA, (i) Line plot for region of interest (ROI), (white dashed line shows data extraction location for line plot), (j) FWHM plot corresponding to Figure 6 (i). CAM: combined aperture mask, LAM: lens array mask, DICAM: direct imaging with combined aperture mask, LRRA: Lucy-Richardson-Rosen algorithm, ORI: object response intensity, SCOPE: super-resolution correlating optical endoscopy, FWHM: full-width half maximum.

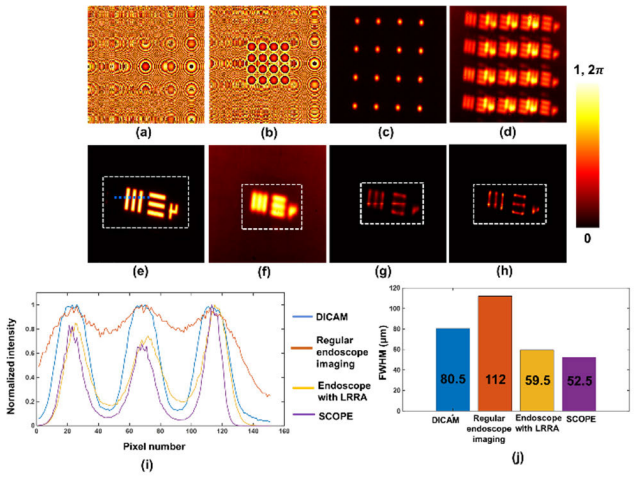

FIGURE 7. Experimental results for multielement object (O2). (a) CAM (4 × 4), (b) LAM (4 × 4), (c) recorded PSF using LAM, (d) recorded ORI using LAM, (e) ORI using CAM, (f) ORI for regular endoscope, (g) regular endoscopy using LRRA, (h) SCOPE using LRRA, (i) Line plot for Region of Interest (ROI), (blue dashed line shows data extraction location for line plot), (j) FWHM plot corresponding to Figure 7 (i), CAM: Combined Aperture Mask, LAM: Lens Array Mask, DICAM: Direct Imaging with Combined Aperture Mask, LRRA: Lucy-Richardson-Rosen Algorithm, ORI: Object Response Intensity, SCOPE: Super-resolution Correlating Optical Endoscopy, FWHM: Full-Width Half Maximum).

regular endoscope imaging and SCOPE for O2 using LRRA are depicted in Figure 7(g, h). On comparing Figures 7(e-h), it is clear that all three elements (vertical, horizontal gratings, digit 4) are best resolved in the case of SCOPE. Furthermore, the line plot shown in Figure 7(i) along the vertical grating of the highlighted region confirms the resolution enhancement for SCOPE compared to direct endoscope recording. Furthermore, the FWHM was calculated from the plots in

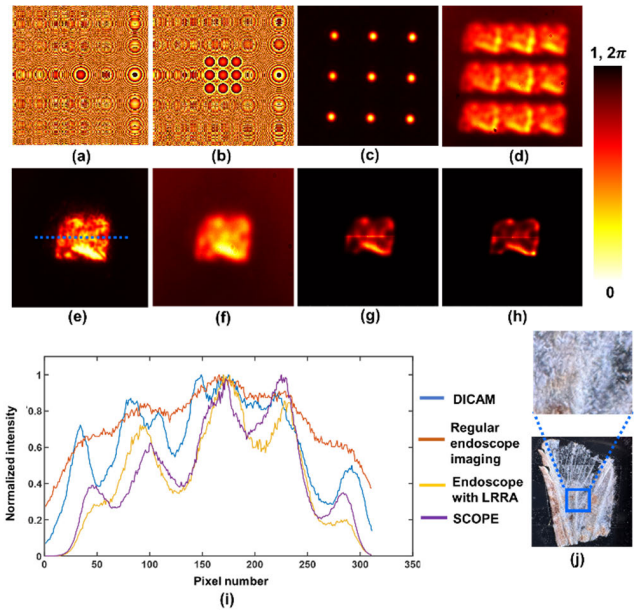

FIGURE 8. Experimental results for the biological sample (O3). (a) CAM (3 × 3), (b) LAM (3 × 3), (c) recorded PSF using LAM, (d) recorded ORI using LAM, (e) ORI using CAM, (f) ORI for regular endoscopy, (g) regular endoscopy using LRRA, (h) SCOPE using LRRA, (i) Line plot for Region of Interest (ROI), (blue dashed line shows data extraction location for line plot), (j) Actual photograph of biological sample (blue box represents the ROI and magnified version of ROI is shown in its top). CAM: combined aperture mask, LAM: lens array mask, DICAM: direct imaging with combined aperture mask, LRRA: Lucy-Richardson- Rosen algorithm, ORI: object response intensity, SCOPE: super-resolution correlating optical endoscopy.

Figure 7 (i) and is shown in Figure 7 (j). The minimum value of the FWHM was obtained in SCOPE compared to the other methods for O2.

Finally, SCOPE was implemented for O3, i.e., a real biological sample (insect wing). We recorded PSFs and ORIs for O3 similar to those for O1 and O2, and the corresponding results are shown in Figure 8. Figure 8(a-d) shows the (a) CAM (3 × 3), (b) LAM (3 × 3), (c) recorded PSF for the LAM, and (d) ORI for the LAM. The recorded ORIs for the CAM and ORIs for direct recording via regular endoscopy are presented in Figure 8(e, f), respectively. The reconstruction results for regular endoscope imaging and SCOPE for O3 using LRRA are depicted in Figure 8(g, h). A comparative analysis of Figure 8(e-h) shows enhanced spatial features of O3 using SCOPE compared to direct endoscope recording. A line plot for the ROI (along the blue dashed line) for Figure 8(e-h) is shown in Figure 8(i) to indicate the resolution enhancement of O3 using SCOPE. Figure 8 (j) shows an actual photograph of a biological sample (the blue box represents the ROI, and a magnified version of the ROI is shown at the top). For this entire experimental study, LRRA was performed under the following conditions ($\alpha = 0.4$, $\beta = 1$, $40 \leq n \leq 55$), where n is the number of iterations.

V. DISCUSSION

SCOPE has been developed to non-invasively improve the resolution limit of commercial endoscopes. The preliminary

results are promising. In general, the diagnostician manoeuvres the endoscope through the human body using an angulation controller, which consists of many wires that are connected to the tip of the endoscope system [21]. When the angulation controller is adjusted, the wires are pulled, causing a turn in the tip of the endoscope system. Most commercial endoscopy systems consist of *x*-*y* controls that allow the diagnostician to manoeuvre the tip of the probing unit along different directions to follow through the turns of the gastrointestinal tract. However, this conventional manoeuvring causes an additional linear phase in the spatial spectrum. This linear phase is important because it shifts the image in the image sensor. However, this shift does not affect the resolution as long as the PSF experiences the same shift. An ideal scenario would be that the diagnostician clicks the SCOPE recording function and the tip of the endoscope moves to predefined locations without tilting, acquiring multiple images of the object. The recordings are processed in real time, and the reconstruction result is shown to the diagnostician, which is possible with the current solutions for computation, sensing and angulation control. In this study, we presented the results for 9 camera shots (3×3) and 16 camera shots (4×4). However, it is possible to record different numbers of images while scanning, for example, 25 camera shots (5×5). As we increase the number of recordings during scanning as much as possible, better noise suppression and resolution enhancement can be obtained.

VI. CONCLUSION

In this study, a Super-resolution Correlating OPtical Endoscopy (SCOPE) system is proposed and demonstrated through both simulation studies and proof-of-concept experiments. SCOPE is based on the principle of I-COACH and involves noise averaging to achieve super-resolution. Enhanced resolution can be achieved by imaging an object over time at multiple locations around the object. In SCOPE, image arrays of sizes (3×3) and (4×4) of objects (O1, O2, and O3) were recorded using LAM, processed with an identical PSF array and reconstructed using the LRRA algorithm. The reconstruction results demonstrate an enhanced resolution for SCOPE compared to individual recordings. We believe that the developed technique can be quickly absorbed into commercial endoscopy systems to achieve super-resolution imaging.

ACKNOWLEDGMENT

(Oskar Tamm, Vipin Tiwari, and Shivasubramanian Gopinath contributed equally to this work.)

REFERENCES

[1] Y. Tang, S. Anandasabapathy, and R. Richards-Kortum, "Advances in optical gastrointestinal endoscopy: A technical review," *Mol. Oncol.*, vol. 15, no. 10, pp. 2580–2599, Sep. 2020.
[2] H. J. Trussell and M. J. Vrhel, *Fundamentals of Digital Imaging*. Cambridge, U.K.: Cambridge Univ. Press, 2008.
[3] P. Suetens, *Fundamentals of Medical Imaging*, 2nd ed. Cambridge, U.K.: Cambridge Univ. Press, 2009.
[4] E. Hecht, *Optics*. London, U.K.: Pearson, 2012.
[5] L. Fu and M. Gu, "Fibre-optic nonlinear optical microscopy and endoscopy," *J. Microsc.*, vol. 226, no. 3, pp. 195–206, Jun. 2007.
[6] M. J. Gora, M. J. Suter, G. J. Tearney, and X. Li, "Endoscopic optical coherence tomography: Technologies and clinical applications [Invited]," *Biomed. Opt. Exp.*, vol. 8, no. 5, p. 2405, Apr. 2017.
[7] L. R. Fisher and W. L. Hasler, "New vision in video capsule endoscopy: Current status and future directions," *Nature Rev. Gastroenterol. Hepatol.*, vol. 9, no. 7, pp. 392–405, May 2012.
[8] B. A. Flusberg, E. D. Cocker, W. Piyawattanametha, J. C. Jung, E. L. M. Cheung, and M. J. Schnitzer, "Fiber-optic fluorescence imaging," *Nature Methods*, vol. 2, no. 12, pp. 941–950, Nov. 2005.
[9] P. Caramazza, O. Moran, R. Murray-Smith, and D. Faccio, "Transmission of natural scene images through a multimode fibre," *Nature Commun.*, vol. 10, no. 1, p. 2029, May 2019.
[10] W. Choi, M. Kang, J. H. Hong, O. Katz, B. Lee, G. H. Kim, Y. Choi, and W. Choi, "Flexible-type ultrathin holographic endoscope for microscopic imaging of unstained biological tissues," *Nature Commun.*, vol. 13, no. 1, p. 4469, Aug. 2022.
[11] V. Anand and J. Rosen, "Interferenceless coded aperture correlation holography—A new technique for recording incoherent digital holograms without two-wave interference," *Opt. Exp.*, vol. 25, no. 12, pp. 13883–13896, Jun. 2017.
[12] J. Rosen, A. Vijayakumar, M. Kumar, M. R. Rai, R. Kelner, Y. Kashter, A. Bulbul, and S. Mukherjee, "Recent advances in self-interference incoherent digital holography," *Adv. Opt. Photon.*, vol. 11, no. 1, pp. 1–66, Feb. 2019.
[13] J. Rosen, V. Anand, and N. Hai, *Digital Holography Based on Aperture Engineering*. Bellingham, WA, USA: SPIE, 2023.
[14] J. Rosen and V. Anand, "Optical imaging using coded aperture correlation holography (COACH) with PSF of spatial-structured longitudinal light beams—A study review," *Photonics*, vol. 11, no. 2, p. 115, Feb. 2024.
[15] N. Dubey, J. Rosen, and I. Gannot, "High-resolution imaging system with an annular aperture of coded phase masks for endoscopic applications," *Opt. Exp.*, vol. 28, no. 10, pp. 15122–15137, May 2020.
[16] V. Anand, M. L. Han, J. Maksimovic, S. H. Ng, T. Katkus, A. R. Klein, K. R. Bambery, M. J. Tobin, J. P. Vongsvivut, and J. Juodkazis, "Single-shot mid-infrared incoherent holography using Lucy-Richardson-Rosen algorithm," *Opto-Electron. Sci.*, vol. 1, no. 3, Jan. 2022, Art. no. 210006.
[17] A Jayavel, S. Gopinath, P. P. Angamuthu, F. G. Arockiaraj, A. Bleahu, A. P. I. Xavier, D. Smith, M. Han, I. Slobozhan, S. H. Ng, and T. Katkus, "Improved classification of blurred images with deep-learning networks using Lucy-Richardson-Rosen algorithm," *Photonics*, vol. 10, no. 4, p. 396, Apr. 2023.
[18] P. A. Praveen, F. G. Arockiaraj, S. Gopinath, D. Smith, T. Kahro, S.-M. Valdma, A. Bleahu, S. H. Ng, A. N. K. Reddy, T. Katkus, A. S. J. F. Rajeswary, R. A. Ganeev, S. Pikker, K. Kukli, A. Tamm, S. Juodkazis, and V. Anand, "Deep deconvolution of object information modulated by a refractive lens using Lucy-Richardson-Rosen algorithm," *Photonics*, vol. 9, no. 9, p. 625, Aug. 2022.
[19] J. Rosen and V. Anand, "Incoherent nonlinear deconvolution using an iterative algorithm for recovering limited-support images from blurred digital photographs," *Opt. Exp.*, vol. 32, no. 1, pp. 1034–1046, Jan. 2024.
[20] W. Zhao et al., "Sparse deconvolution improves the resolution of live-cell super-resolution fluorescence microscopy," *Nature Biotechnol.*, vol. 40, pp. 606–617 Nov. 2022.
[21] E. Rozeboom, J. Ruiter, M. Franken, and I. Broeders, "Intuitive user interfaces increase efficiency in endoscope tip control," *Surgical Endoscopy*, vol. 28, no. 9, pp. 2600–2605, Mar. 2014.

OSKAR TAMM is currently pursuing the bachelor's degree. He is also a Lab Assistant with the CIPHR Research Group, Institute of Physics, University of Tartu, Estonia. His research interests include astronomy, imaging, holography, and computational optics. He has completed internship and training from Karl Storz Video Endoscopy, Estonia.

VIPIN TIWARI received the Ph.D. degree in physics (applied optics) from Kumaun University, India, in 2023. Later, he was an International Visiting Researcher with Chiba University, Japan. He is currently an Early Career Researcher in optics and photonics. He is also a Postdoctoral Research Fellow with the CIPHR Research Group, Institute of Physics, University of Tartu, Estonia. He has published several notable journal articles, conference proceedings, and book chapter in prestigious journals and conferences in optics and photonics. His current research interests include computational imaging, polarization imaging, and digital holography. He is a member of Optica.

SHIVASUBRAMANIAN GOPINATH received the bachelor's and master's degrees in physics from the Thiagarajar College, India, in 2020 and 2022, respectively. He is currently pursuing the Ph.D. degree. He is also a Junior Research Fellow with the Institute of Physics, University of Tartu, Estonia. In the Ph.D. topic, he is also working on developing new imaging technologies using an ensemble of self-interfering beams. His research outputs have been highlighted in IEEE Spectrum and Phy.Org. He has coauthored and published more than 15 articles and conference proceedings. His research interests include computational imaging, incoherent digital holography, coded aperture imaging, and diffractive optics. He is also a member of the CIPHR Research Group, Institute of Physics. He was awarded the best outgoing student from the Institute of Physics.

ARAVIND SIMON JOHN FRANCIS RAJESWARY received the master's degree in computer applications from Manonmaniam Sundaranar University, India, in 2005. He is currently the Research Manager of the CIPHR Research Group, Institute of Physics, University of Tartu, Estonia. He has coauthored 30 journal articles and conference proceedings. His research interests include optical experiments, deep learning, and software development.

SCOTT AROCKIA SINGH received the Graduate degree from the Stanley Medical College, India, in 1997. He is currently the Chairperson and the Managing Director of Dr. Scott's Laser Piles, Fistula Laparoscopic Center and Consultant Laparoscopic, Dr. Jeyasekharan Hospital, Nagercoil, Tamil Nadu, India. He has more than 20 years of experience as a Surgeon and performed more than 5000 successful surgeries. He holds a Fellowship from the Royal College of Surgeons of Edinburgh, U.K. He is also a Professor in surgery with the National Board of Examination, New Delhi. His areas of expertise are laser piles surgery, laser hemorrhoidoplasty, laser fissure surgery, laser fistula surgery, laparoscopic cholecystectomy, appendicectomy, hernia repair, and hysterectomy. He has several publications in national and international journals. He is a Life Member of Indian Association of Gastrointestinal Endoscopic Surgeons, the Association of Surgeons of India, Indian Medical Association, and the Association of Colorectal Surgeons of India.

JOSEPH ROSEN is currently the Benjamin Swig Professor in optoelectronics with the School of Electrical and Computer Engineering, Ben-Gurion University of the Negev, Be'er-Sheva, Israel. He has coauthored more than 300 publications. His research interests include digital holography, optical microscopy, diffractive optics, statistical optics, biomedical optics, optical computing, and image processing. He is a fellow of SPIE and Optica [formerly the Optical Society of America (OSA)].

VIJAYAKUMAR ANAND is currently the ERA Chair and an Associate Professor in computational imaging with the CIPHR Research Group, Institute of Physics, University of Tartu, Estonia. He is also an Adjunct Associate Professor with the Optical Sciences Center, Swinburne University of Technology, Australia. He has coauthored more than 150 publications. His research interests include digital holography, diffractive optics, lithography, and computational imaging. He is a Senior Member of Optica (formerly the Optical Society of America).